Groundwater-native Fe(II) oxidation prior to aeration with H_2O_2 to enhance As(III) removal

Roy, Mrinal; van Genuchten, Case M.; Rietveld, Luuk; van Halem, Doris

Citation (APA)

Important note
To cite this publication, please use the final published version (if applicable).
Please check the document version above.

Groundwater-native Fe(II) oxidation prior to aeration with H_2O_2 to enhance As(III) removal

Mrinal Roy [a],[*], Case M. van Genuchten [b], Luuk Rietveld [a], Doris van Halem [a]

[a] *Water Management Department, Faculty of Civil Engineering and Geosciences, Delft University of Technology, Stevinweg 1, Delft CN 2628, the Netherlands*
[b] *Department of Geochemistry, Geological Survey of Denmark and Greenland, Copenhagen DK 1350, Denmark*

ARTICLE INFO

ABSTRACT

Groundwater contaminated with arsenic (As) must be treated prior to drinking, as human exposure to As at toxic levels can cause various diseases including cancer. Conventional aeration-filtration applied to anaerobic arsenite (As(III)) contaminated groundwater can remove As(III) by co-oxidizing native iron (Fe(II)) and As(III) with oxygen (O_2). However, the As(III) removal efficiency of conventional aeration can be low, in part, because of incomplete As(III) oxidation to readily-sorbed arsenate (As(V)). In this work, we investigated a new approach to enhance As(III) co-removal with native Fe(II) by the anaerobic addition of hydrogen peroxide (H_2O_2) prior to aeration. Experiments were performed to co-oxidize Fe(II) and As(III) with H_2O_2 (anaerobically), O_2 (aerobically), and by sequentially adding of H_2O_2 and O_2. Aqueous As(III) and As(V) measurements after the reaction were coupled with solid-phase speciation by Fe and As K-edge X-ray absorption spectroscopy (XAS). We found that complete anaerobic oxidation of 100 μM Fe(II) with 100 μM H_2O_2 resulted in co-removal of 95% of 7 μM As (III) compared to 44% with 8.0-9.0 mg/L dissolved O_2. Furthermore, we found that with 100 μM Fe(II), the initial Fe(II):H_2O_2 ratio was a critical parameter to remove 7 μM As(III) to below the 10 μg/L (0.13 μM) WHO guideline, where ratios of 1:4 (mol:mol) Fe(II):H_2O_2 led to As(III) removal matching that of 7 μM As(V). The improved As (III) removal with H_2O_2 was found to occur partly because of the well-established enhanced efficiency of As(III) oxidation in Fe(II)+H_2O_2 systems relatively to Fe(II)+O_2 systems. However, the XAS results unambiguously demonstrated that a large factor in the improved As(III) removal was also due to a systematic decrease in crystallinity, and thus increase in specific surface area, of the generated Fe(III) (oxyhydr)oxides from lepidocrocite in the Fe(II)+O_2 system to poorly-ordered Fe(III) precipitates in the Fe(II)+H_2O_2 system. The combined roles of H_2O_2 (enhanced As(III) oxidation and structural modification) can be easily overlooked when only aqueous species are measured, but this dual impact must be considered for accurate predictions of As removal in groundwater treatment.

1. Introduction

An estimated 94-220 million people are exposed to naturally occurring arsenic (As) in groundwater (mainly as arsenite (As(III))) at levels above the World Health Organization (WHO) drinking water guideline of 10 μg/L (0.13 μM) (Podgorski and Berg, 2020). Exposure to As-contaminated water can pose major threats to human health causing diseases such as skin, bladder and lung cancers, reproductive disorders, and neuro-developmental problems in children (Kapaj et al., 2006; Tseng, 1977). Therefore, it is crucial that groundwater contaminated with toxic levels of As be treated prior to drinking.

Conventional aeration-filtration is a common treatment method that involves aerating anaerobic As(III)-rich groundwater that contains co-occurring iron (Fe(II)), followed by filtration of the generated solids (Gude et al., 2016; Hug and Leupin, 2003; Roberts et al., 2004). This method relies on As(III) and Fe(II) co-oxidation by O_2 to form particulate Fe(III) (oxyhydr)oxides (or Fe solids) that can bind As (Bora et al., 2016; Gude et al., 2016). Compared to other techniques, aeration-filtration is advantageous as it is economically attractive, no dosing of chemicals is required, it removes various groundwater contaminants (Fe(II), ammonium, manganese) simultaneously, and it generates biologically stable drinking water (low in nutrients), thereby ensuring microbial safety in distribution networks (Annaduzzaman et al., 2021a; Gude et al., 2017). While conventional aeration-filtration is applied widely in

---

groundwater treatment and Fe solids are very good adsorbents for As, this conventional approach can be ineffective for As(III) removal, which often demands additional dosing of Fe to meet drinking water guidelines (Annaduzzaman et al., 2018; Annaduzzaman et al., 2021b; Sharma et al., 2016). For example, previous studies have shown that co-removal of As(III) with Fe(II) through aeration-filtration only yields between 8-50% removal, depending on the initial As concentration, As:Fe ratio, and the presence of other competing ions (i.e. manganese, phosphate) (van Genuchten and Ahmad, 2020; Holm and Wilson, 2006; Li et al., 2016).

The low efficacy of As(III) co-removal with native Fe(II) during aeration-filtration can be due to several factors. First, Fe solids generated by aeration (by O_2) can be moderately crystalline (Ahmad et al., 2019) with a lower reactive specific surface area than the poorly-ordered Fe solids generated with stronger oxidants, such as HOCl and $KMnO_4$ (Ahmad et al., 2019). Second, Fe solids have orders of magnitude lower sorption affinity for As(III) than oxidized arsenate (As(V)) and As(III) oxidation during aeration is slow and partial (Bissen and Frimmel, 2003; Gude et al., 2017; Roberts et al., 2004). Third, the relatively high pH resulting from $CO_{2(g)}$ degassing during groundwater aeration creates a less favourable environment for As(V) adsorption (Annaduzzaman et al., 2021b; Dixit and Hering, 2003), which can be minimized by avoiding aeration. Thus, the co-removal of groundwater As(III) with native Fe(II) can be optimized by forming poorly-ordered solids, with high reactive surface area, and by co-oxidizing As(III) effectively and rapidly prior to aeration to minimize pH increase induced by $CO_{2(g)}$ efflux.

The addition of hydrogen peroxide (H_2O_2) is an attractive option for anaerobic As(III) and Fe(II) co-oxidation because H_2O_2 reacts rapidly with Fe(II), and is relatively inexpensive to generate on- or off-site, and is considered a green alternative to harsher chemical oxidants because of its non-toxic reaction products (Bandaru et al., 2020; Pham et al., 2012a, 2012b). Additionally, H_2O_2 is an intermediate formed during Fe(II) oxidation by O_2 (Hug and Leupin, 2003) and may as such be considered a natural additive in anaerobic groundwater treatment. In principle, the presence of H_2O_2 in As(III) and Fe(II)-rich solutions is beneficial because it oxidizes Fe(II) at a rate four orders of magnitude higher than O_2 (Bandaru et al., 2020; King and Farlow, 2000; King, 1998), which can result in the generation of poorly-ordered Fe(III) solids (Bandaru et al., 2020; van Genuchten and Peña, 2017). In addition, while direct As(III) oxidation by H_2O_2 is kinetically limited, the oxidation of Fe(II) by H_2O_2 leads to a high stoichiometric yield of reactive oxygen species (ROS), such as *OH or Fe(IV), that can effectively oxidize As(III) (Hug and Leupin, 2003). The theoretical ROS yield per mol of oxidized Fe(II) is 1:1 for H_2O_2 compared to 1:3 for O_2 (Hug and Leupin, 2003), which would translate to more As(III) co-oxidation per mole of oxidized Fe(II) if H_2O_2 is applied. While Fenton-type systems (i.e. those containing Fe(II)+ H_2O_2) have been investigated in the context of As(III) removal previously (Bandaru et al., 2020; Catrouillet et al., 2020), most studies performed, are over-dosing H_2O_2 in solutions open to the atmosphere, initially containing O_2. Careful control of the H_2O_2 input and thus the Fe (II):H_2O_2 ratio, could thus be more effective, particularly in the case of treating anaerobic groundwater, because it can optimize the use of natural Fe(II), minimize the consumption of H_2O_2, and can avoid an increase in pH due to $CO_{2(g)}$ efflux.

In this study a novel approach is therefore proposed to enhance As (III) removal in groundwater with the native Fe(II), through anaerobic oxidation of the native Fe(II) by H_2O_2 prior to aeration. Moreover, we compared the impact of oxidizing Fe(II) with O_2 (aerobically), H_2O_2 (anaerobically), and sequentially with H_2O_2 (anaerobically) followed by O_2 (aerobically) on As(III) removal. The reactions were tracked by aqueous As(III) and As(V) speciation measurements and by characterization of the solid reaction products by synchrotron-based Fe and As K-edge X-ray absorption spectroscopy (XAS). In addition, we examined the impact of under- and over-dosage of H_2O_2 (anaerobically) on the extent of Fe(II) and As(III) co-oxidation. Finally, we validated this approach by studying H_2O_2 addition to Fe(II)-containing raw anaerobic groundwater

2. Materials and methods

2.1. Chemicals

Ultrapure water (18.2 mΩ.cm) was used to prepare all experimental solutions and was spiked with to 2.5 mM $NaHCO_3$ and 10 mM NaCl by dissolving 0.32 g of sodium bicarbonate (J.T. Baker™) and 0.88 g of sodium chloride (J.T. Baker™) in 1.5 L. The concentration of $NaHCO_3$ (2.5 mM) and NaCl (10 mM) were selected to achieve an alkalinity and conductivity (990 µS/cm) similar to previous studies in synthetic groundwater (Ahmad et al., 2019; van Genuchten et al., 2012). As(III), As(V), and Fe(II) were added from stock solutions, which were freshly prepared daily. Stock solutions were generated by dissolving defined amounts of sodium (meta)arsenite ($NaAsO_2$) or sodium arsenate dibasic heptahydrate ($Na_2HAsO_4.7H_2O$) (Sigma-Aldrich) to ultrapure water and ferrous sulfate heptahydrate ($FeSO_4.7H_2O$) (Sigma-Aldrich)) to 1 mM HCl respectively. H_2O_2 stock solutions were also freshly diluted with defined volumes of the 30% w/w H_2O_2 solution (Sigma-Aldrich) in ultrapure water. For pH adjustment, 1 M HCl or 1 M NaOH (Merck Millipore) was used.

2.2. Experimental setup and procedure

The experiments were conducted at room temperature (20±3 °C) in 2 L glass jars with perforated lids (Fig. S1). The jars initially contained 1 L of ultrapure water (18.2 mΩ.cm) with 2.5 mM $NaHCO_3$, 10 mM NaCl, and 7 µM As(III) or As(V). The solution was then purged with $N_{2(g)}$ to obtain dissolved O_2 concentrations of <0.1 mg/L and the pH was set to 7.3-7.5. Next, Fe(II) was added to the O_2-purged solution. The oxidation of Fe(II) was initiated by dosing H_2O_2 or O_2 alone or by sequentially dosing H_2O_2 followed by O_2 (H_2O_2+O_2). To dose O_2, an air-pump was used to raise the dissolved O_2 to 8.0-9.0 mg/L (from initial levels of <0.1 mg/L) after adding Fe(II). The solution was mixed with a magnetic stirrer (LABINCO L23) at 150 rpm for 30 min after Fe(II) oxidation began. In H_2O_2 experiments, $N_{2(g)}$ was continuously purged throughout the mixing period to minimize the impact of atmospheric O_2 influx and to maintain dissolved O_2 levels <0.1 mg/L. For the sequential H_2O_2+O_2 experiments, partial Fe(II) oxidation was performed first by adding H_2O_2 and mixing for 5 min under continuous $N_{2(g)}$ purging (dissolved O_2 <0.1 mg/L), followed by O_2 dosing using the air-pump (dissolved O_2 = 8.0-9.0 mg/L) for the remaining 25 min. The pH of all solutions was maintained between 7.3-7.5 during experiments by manual additions of 1 M NaOH or 1 M HCl. The pH and dissolved O_2 were monitored using a multimeter (WTW™ MultiLine™ Multi 3630 IDS).

2.3. Experimental conditions

To determine the impact of various Fe(II) oxidant conditions on As (III) co-removal, experiments were performed in the H_2O_2, O_2, and sequential H_2O_2+O_2 systems by completely oxidizing 100 µM Fe(II) with 100 µM H_2O_2 (anaerobically), 8.0-9.0 mg/L O_2 (aerobically), or sequentially by 5, 10, 20, or 40 µM H_2O_2 (anaerobically) followed by O_2 (aerobically). Another set of experiments was performed to examine the effect of H_2O_2 concentration (and thus Fe(II):H_2O_2 ratio) on the co-oxidation and removal of 100 µM Fe(II) and 7 µM As(III). For these experiments, the H_2O_2 concentrations (i.e. 10, 20, 40, 60, 100, 200, 300, and 400 µM) were selected to span the stoichiometric amount required for total Fe(II) oxidation. A set of experiments was also repeated with initial 7 µM As(V) in place of As(III). In addition to laboratory tests, experiments were performed using raw Dutch groundwater, which was obtained directly from the influent of a drinking water treatment plant. For these experiments, the raw anaerobic water (initial composition given in Table S1) was spiked with 7 µM As(III). The removal of As(III) was investigated by completely oxidizing the groundwater-native Fe(II) with either H_2O_2 or O_2. In the H_2O_2 experiments with raw groundwater, $N_{2(g)}$ was not used to decrease the dissolved O_2 to <0.1 mg/L. All

experiments were replicated at least twice. A schematic overview of the experimental conditions is shown in Fig. S1.

2.4. Chemical analysis

During the 30 min reaction time, filtered and unfiltered water samples were collected at 0, 2, 5, 10, 20, and 30 min. Filtration was performed with 0.2 μm polyethersulfone filters (Macherey-Nagel GmbH & Co. KG). Immediately after collection, the samples were acidified with 1% (v/v) ultrapure nitric acid (ROTIPURAN® Ultra 69%) to stop further reactions and dissolve any solids. Acidified samples were stored at 4 °C until analysis. We refer to Fe measured in the filtered solution as Fe(II), which we verified by measuring Fe(II) in a subset of filtered samples using an Fe cell test kit (Merck Millipore). For dissolved As speciation, we followed the approach described in Gude et al. (2018), which is based on using an anionic exchange resin (Amberlite* IRA-402 chlorite) to separate non-ionic As(III) and negatively-charged As(V). The unfiltered samples were used to determine the total Fe and Fe(III) concentration, where the difference between total Fe and dissolved Fe represented the Fe(III). The samples were analyzed for As and Fe (in triplicates) by inductively coupled plasma mass spectrometry (ICP-MS, Analytikal Jena model PlasmaQuant MS).

2.5. X-ray absorption spectroscopy

2.5.1. Data collection

Solids for XAS analysis were collected using filter papers at the end of the oxidation experiments. The filter papers with solids attached were stored at -80 °C before affixing the sample (filter and solids) to custom sample holders using Kapton tape. Fe and As K-edge XAS data were collected at beam line 2–2 of the Stanford Synchrotron Radiation Lightsource (SSRL, Menlo Park, USA). Fe K-edge XAS data were recorded at room temperature out to $k = 13$ Å^{-1} and As K-edge XAS data were recorded at liquid nitrogen temperatures ($\approx$80 °K) in fluorescence mode out to $k = 14$ Å^{-1}. For beam calibration, the maximum of the first derivative of Fe(0) and Au(0) foils was set to 7112 eV and 11919 eV for Fe and As data, respectively. Spectral alignment, averaging and background subtraction of individual spectra were performed using SixPack software (Webb, 2005), following standard procedures described in van Genuchten et al. (2012). Extraction of the Fe K-edge EXAFS spectra was performed using k^3-weighting and the Fe K-edge EXAFS spectra were Fourier-transformed over the k-range 2 to 11 Å^{-1} using a Kaiser-Bessel window with dk of 3 Å^{-1}.

2.5.2. Data analysis

The Fe K-edge EXAFS spectra were analysed by liner combination fits (LCFs) ($k = 2$-11 Å^{-1}) with the SixPack software (Webb, 2005) using the EXAFS spectra of three reference Fe(III) (oxyhydr)oxides: moderately crystalline lepidocrocite (Lp), nanocrystalline 2-line ferrihydrite (2LFh), and highly disordered oxyanion-rich hydrous ferric oxide (oxy-HFO). These three reference Fe(III) (oxyhydr)oxides were selected based on previous studies that report these references reproduced the Fe(III) solids generated by Fe(II) oxidation using a range of chemical oxidants (Ahmad et al., 2019; van Genuchten et al., 2018; van Genuchten et al., 2014). The fraction of the three references in each experimental sample derived from the LCFs was normalized to one.

The As K-edge XANES spectra were analyzed by LCFs using SixPack software to determine the fraction of adsorbed As(III) and As(V). The LCFs were performed with a fit range of 11860 to 11880 eV using reference spectra of As(III) and As(V) adsorbed to 2-line ferrihydrite. In the LCFs, negative fractions of the reference spectra were not allowed and the component sum was not constrained to 1. The concentration of adsorbed As(III) and As(V) was calculated by multiplying the LCF-derived fraction of As(III) and As(V) by the concentration of total As removed from solution determined by ICP-MS. We use the As K-edge XAS data primarily to determine the oxidation state of As bound to the

solid phase. Shell-by-shell fits of the EXAFS spectra were not performed partly because many of our samples contained multiple As oxidation states, which complicates the interpretation of shell fits (van Genuchten et al., 2012; van Genuchten and Ahmad, 2020). Further details on XAS sample preparation and data collection are given in the Supplementary Materials.

3. Results and discussion

3.1. Solid-phase Fe structure and its relation to Fe(II) oxidation kinetics

Fig. 1(A) and (B) shows the Fe K-edge EXAFS spectra, and corresponding Fourier transforms, of the three reference Fe(III) (oxyhydr) oxides and the experimental samples generated in the O_2, H_2O_2, and sequential $H_2O_2+O_2$ systems. Comparing the EXAFS spectral features of Lp, 2LFh, and oxy-HFO, a peak can be observed in Lp near 7.84 Å^{-1}, which dampened in 2LFh and disappeared in oxy-HFO. In addition, the first oscillation from 4-5 Å^{-1} is asymmetric in Lp but becomes more symmetric for 2LFh and oxy-HFO, with the oscillations at k > 8 Å^{-1} becoming more broad with lower amplitude from Lp to 2LFh to oxy-HFO. These features are consistent with a progressive decrease in structural order from Lp to 2LFh to oxy-HFO (Toner et al., 2009; van Genuchten et al., 2012). Visual comparison of the EXAFS spectra of the experimental solids indicates that the EXAFS spectrum of the sample generated by O_2 oxidation closely matched the line shape and phase of the Lp EXAFS spectrum. However, a gradual and systematic shift in EXAFS features from Lp to 2LFh and oxy-HFO was observed with an increasing concentration of initial H_2O_2, and thus increasing fraction of Fe(II) oxidized by H_2O_2. As shown in the Fourier-transform (Fig. 1(B)), these changes in the EXAFS spectra of the samples correspond to a systematic decrease in the amplitude of second-shell peak, which arises from Fe-Fe atomic pairs, suggesting a progressive decrease in structural order with increasing H_2O_2 concentration (Toner et al., 2009; van Genuchten et al., 2012). We assign the second-shell peak with Fe-Fe atomic pairs because no other atoms can be present in the second shell of Fe at high enough concentrations to contribute significantly to this peak (i.e., As can occur in the second shell, but its concentration in the solid phase is too low to be detected in the Fe data).

The LCFs of the EXAFS spectra (Fig. 1(C); Table S2) confirmed the decrease in Fe(III) precipitate crystallinity with increasing initial H_2O_2 concentration. The LCFs indicated that the highest fraction of moderately crystalline Lp was present in the sample generated by O_2 oxidation of Fe(II). The fraction of Lp in the solids derived by LCFs decreased systematically in favor of poorly-ordered Fe(III) precipitates (2LFh and oxy-HFO) with increasing Fe(II) oxidation by H_2O_2. Lp was not detected in the experiments where 100% of Fe(II) was oxidized by H_2O_2. Instead, the solids generated by Fe(II) oxidation with H_2O_2 consisted of 100% poorly-ordered Fe(III) precipitates (Fig. 1(C); Table S2). Such formation of a higher fraction of poorly-ordered Fe solids with H_2O_2 compared to O_2 is consistent with the previously reported impact of Fe(II) oxidation rate on Fe(III) precipitate structure (Ahmad et al., 2019; Bandaru et al., 2020; Catrouillet et al., 2020; van Genuchten and Peña, 2017). The low oxidation rate of Fe(II) with O_2 allows the presence of aqueous Fe(II) to catalyze the crystallization of freshly-precipitated Fe(III) precursors into Lp (Ahmad et al., 2019; Pedersen et al., 2005). By contrast, H_2O_2 oxidizes aqueous Fe(II) too rapidly to permit any Fe(II)-catalyzed crystallization of newly-formed Fe(III) precipitates (Ahmad et al., 2019; Pedersen et al., 2005).

To verify rapid Fe(II) oxidation with H_2O_2, the kinetics of Fe(III) generation was tested over 30 min for the same oxidation conditions (Fig. 1(D)) as used to generate the solids for XAS analysis (i.e. oxidation of 100μM Fe(II) in the O_2, H_2O_2, and $H_2O_2+O_2$ systems). It was observed that all the Fe(II) was oxidized within 10 min regardless of the oxidant (Fig. 1(D)). However, with 100 μM H_2O_2, complete Fe(II) oxidation was faster (<2 min) than with O_2 (between 5-10 min), which is in-line with previous research (Bandaru et al., 2020; King and Farlow, 2000; King,
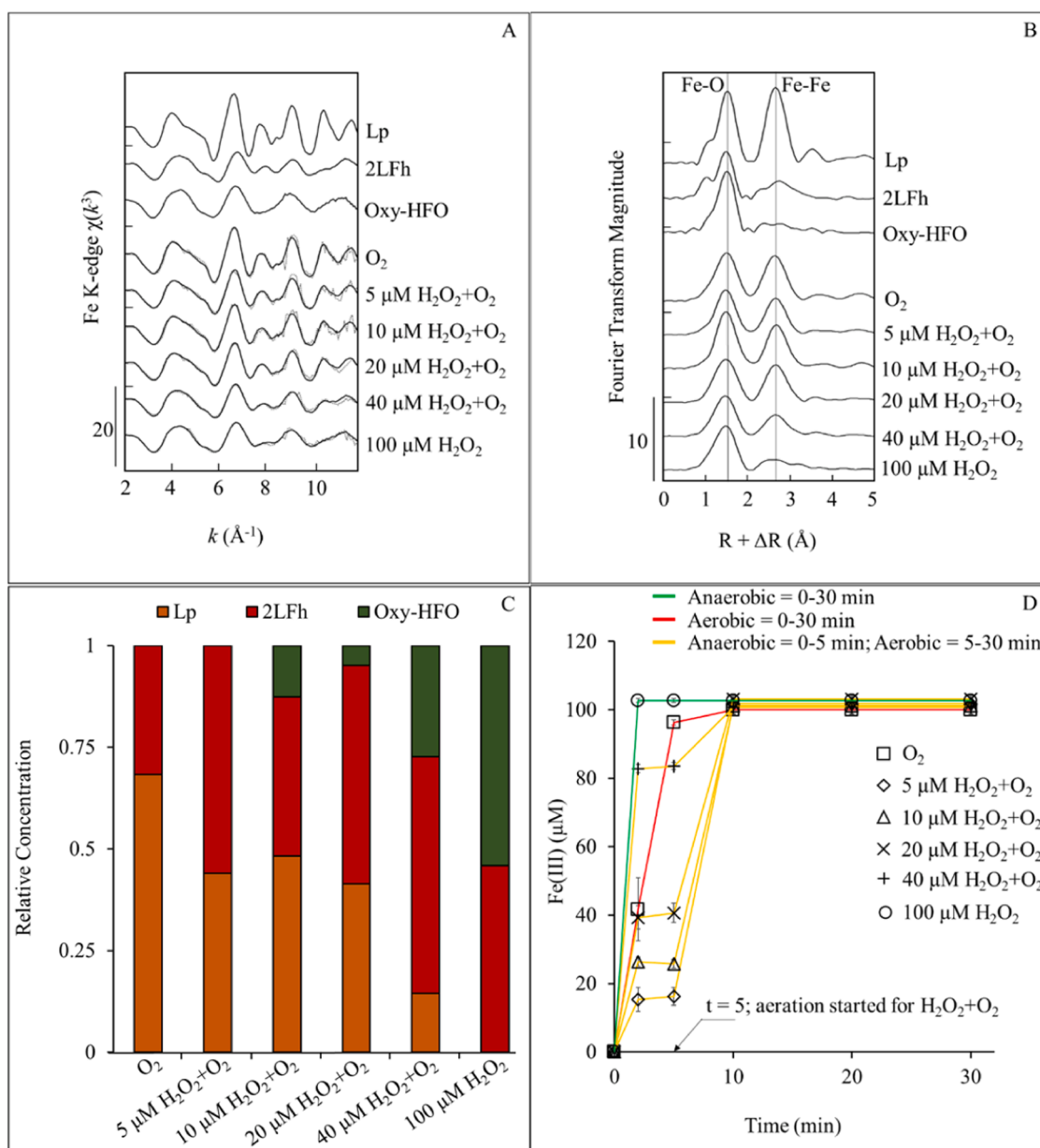
Fig. 1. Fe K-edge EXAFS spectra and corresponding Fourier transforms of the Fe solids (A and B), relative concentration of lepidocrocite (Lp), 2-line ferrihydrite (2LFh), and oxyanion-rich hydrous ferric oxide (oxy-HFO) in the Fe solids determined from LCFs, and kinetics of Fe(III) generation over 30 min when 100 ± 3 μM Fe(II) was oxidized by 8.0-9.0 mg/L O_2 (aerobically; t = 0-30 min), 100 μM H_2O_2 (anaerobically; t = 0-30 min), or sequentially by 5, 10, 20, or 40 μM H_2O_2 (anaerobically; t = 0-5 min) followed by 8.0-9.0 mg/L O_2 (aerobically; t = 5-30 min). The LCF output is overlain on the experimental data in panel A. Solutions initially contained 7 ± 0.5 μM As(III), 2.5 mM $NaHCO_3$, and 10 mM NaCl. All Fe(III) formed solids and no dissolved Fe(III) was detected (data not shown). Data points and error bars represent the average and standard deviation of the samples obtained from replicate experiments.

1998). In the sequential experiments with initial 5, 10, 20 or 40 μM H_2O_2, Fe(II) oxidation was fast but incomplete, with the expected stoichiometric 2:1 mol:mol ratio of Fe(II) oxidation by H_2O_2 observed for all H_2O_2 experiments. This 2:1 stoichiometry led to residual Fe(II) concentrations of 85, 76, 64, and 17 μM at 5 min using H_2O_2 dosages of 5, 10, 20, and 40 μM, respectively, with the remaining Fe(II) oxidized by O_2 added by aeration at t > 5 min. These results show that anaerobic Fe (II) oxidation with H_2O_2 closely followed the expected 2:1 ratio and favoured the formation of poorly-ordered Fe(III) solids, in contrast to O_2, due to its more rapid oxidation rate with Fe(II).

3.2. As(III) removal by Fe solids

Fig. 2(A) shows the co-removal of initial 7 ± 0.5 μM As(III) when

oxidizing 100 ± 3 μM Fe(II) in the O_2, H_2O_2, and sequential H_2O_2+O_2 systems. Comparing the different oxidant conditions, As(III) removal was the lowest in the O_2 system, where the residual dissolved As concentration (t = 30 min) was 3.8 ± 0.2 μM (44% removal). In the sequential H_2O_2+O_2 system, As(III) removal was moderate and the residual dissolved As concentration (t = 30 min) decreased systematically (3.6 ± 0.2, 2.9 ± 0.4, 2.6 ± 0.1, and 1.3 ± 0.10 μM) with increasing initial H_2O_2 concentration (5, 10, 20, and 40 μM H_2O_2). The most removal of initial As(III) was observed using 100 μM H_2O_2, with a residual dissolved As concentration (t = 30 min) of 0.4 ± 0.1 μM (95% removal). Thus, the poorest As removal was observed when Fe(II) was oxidized by O_2 alone and removal increased with an increase in the fraction of Fe(II) oxidized by H_2O_2. This trend is consistent with the increasing fraction of poorly-ordered Fe solids with increasing initial H_2O_2 concentration (Fig. 1(C)),
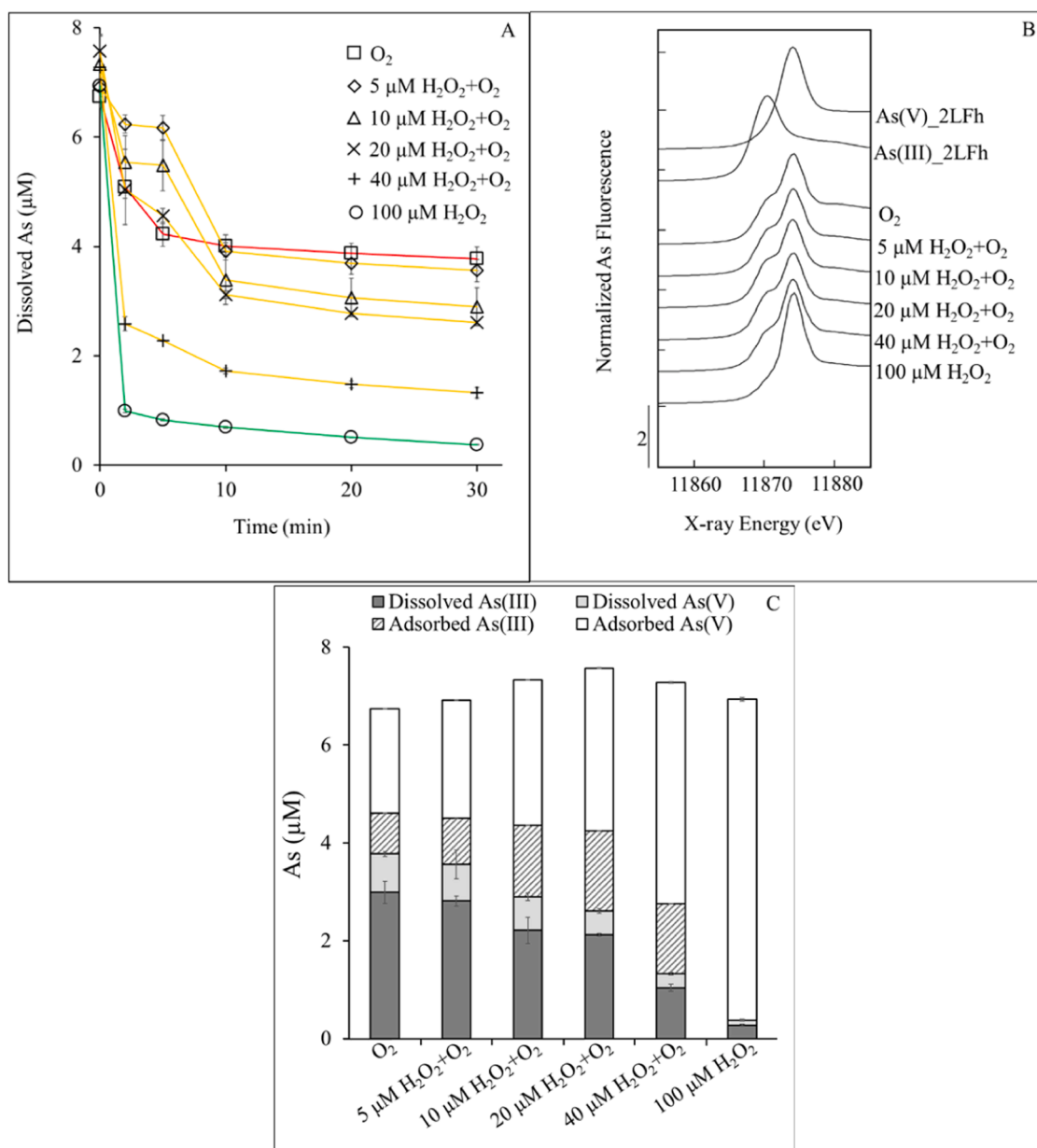
Fig. 2. Removal of initial As(III) over 30 min (A), As K-edge XANES spectra of the generated Fe solids (B), and As speciation at the experiment end ($t = 30$ min) when 100 ± 3 μM Fe(II) was oxidized by 8.0-9.0 mg/L O_2 (aerobically; $t = 0$-30 min) (red line), 100 μM H_2O_2 (anaerobically; $t = 0$-30 min) (green line), or sequentially by 5, 10, 20, or 40 μM H_2O_2 (anaerobically; $t = 0$-5 min) followed by 8.0-9.0 mg/L O_2 (aerobically; $t = 5$-30 min) (yellow line). Solutions initially contained 7 ± 0.5 μM As (III), 2.5 mM NaHCO$_3$, and 10 mM NaCl. Data points and error bars represent the average and standard deviation of the samples obtained from replicate experiments.

as observed in the previous section.

Fig. 2(B) shows the As K-edge XANES spectra of samples generated in the O_2, H_2O_2, and sequential $H_2O_2+O_2$ systems, with the LCFs of the XANES spectra reported in Table S3. The XANES spectra show that As(V) was the dominant species adsorbed on the solids, based on the position of the absorption maximum near 11875 eV. The predominance of solid-phase As(V) was confirmed by the XANES LCFs (Table S3). This suggests effective sorption of As(V) generated via As(III) oxidation by ROS, formed during Fe(II) reactions with both O_2 or H_2O_2, since direct oxidation of As(III) by O_2 or H_2O_2 in the experimental time frame (30 min) was not feasible (Hug and Leupin, 2003).

Combining the aqueous As(III) removal results with the measurements of As oxidation state on the solids (with XANES LCFs) and in solution (with anionic exchange resins) yields the speciation plot given in Fig. 2(C). This plot reveals that, while overall aqueous As(III) removal increased with increasing initial H_2O_2 concentration, the majority of As

bound to the solids was always As(V) and the majority of residual aqueous As was As(III) for all oxidant conditions. For example, in the O_2 system As(V) accounted for 2.2 μM of the total adsorbed As content of 3.0 μM (72%), whereas 80% of the 3.8 μM residual As was As(III). Similarly, in the H_2O_2 system, As(V) was 100% of the adsorbed As and As(III) accounted for 72% of the 0.4 μM residual As. These trends were reproduced in the sequential $H_2O_2+O_2$ system (Fig. 2(C)) and are consistent with the orders of magnitude higher sorption affinity of As(V) than As(III) (Roberts et al., 2004). Although the fraction of As(V) and As (III) bound to the solids was similar among many of the samples, the total amount of oxidized As(III) increased with increasing H_2O_2 concentration (i.e. total As(V) increased from 2.9 μM in the O_2 system to >6 μM in the H_2O_2 system). The increase in As(III) oxidation with H_2O_2 concentration is consistent with more effective ROS generation when Fe (II) is oxidized by H_2O_2 compared to O_2 (Hug and Leupin, 2003), which is attributed to the 1:1 stoichiometric yield of ROS when Fe(II) reacts

with H_2O_2 compared to the 1:3 yield of ROS when Fe(II) reacts with O_2.

Combining the As speciation plots in Fig. 2(C) and the solid-phase Fe speciation plots in Fig. 1(C) uncovers a key finding about the anaerobic co-oxidation of As(III) and Fe(II) by H_2O_2. Comparing the overall As removal between the O_2 experiment and the sequential 40 µM $H_2O_2+O_2$ experiment showed a decrease in the residual As concentration from 3.8 µM to 1.3 µM, a difference of 2.5 µM As when 40 µM H_2O_2 was applied, whereas for the same samples, the total amount of oxidized As(III) was 2.9 µM for the O_2 experiment and 4.8 µM for the sequential 40 µM $H_2O_2+O_2$ experiment, a difference of only 1.9 µM As. The higher overall As removal efficacy for the 40 µM $H_2O_2+O_2$ experiment, cannot be attributed to an increase in As(III) oxidation alone. Therefore, the results indicate that the higher reactive surface area of the poorly-ordered solids generated by Fe(II) oxidation with H_2O_2 played a critical role in improving overall As removal efficacy.

3.3. Under- and over-dosage of H_2O_2

Experiments were performed to identify any benefit from dosing H_2O_2 below or above the stoichiometric amount required to anaerobically oxidize 100±3 µM Fe(II). Fig. 3(A) shows the concentration of oxidized Fe(II) and the corresponding removal of the initial 7±0.2 µM As (III) as a function of different H_2O_2 dosages (10-400 µM) at t = 30 min. As the H_2O_2 concentration increased, the concentration of oxidized Fe (II) also increased up to the complete oxidation of Fe(II) at H_2O_2 concentrations above 60 µM. For H_2O_2 dosages below 60 µM (i.e., under-dosage; 10-40 µM), only partial oxidation of 100±3 µM Fe(II) was observed (20-80% oxidation). However, the ratio of generated Fe(III) to dosed H_2O_2 remained around 2:1 mol:mol for all conditions (Fig. 3(A)), indicating that the 2:1 stoichiometry of Fe(II) oxidation by H_2O_2 was maintained.

The results from the sequential $H_2O_2+O_2$ experiments were consistent with the findings mentioned above. Increasing the H_2O_2 concentration from 10-40 µM, which is below the required amount for 100% Fe (II) oxidation, resulted in improved As removal due to the formation of more Fe(III) precipitates (Section 3.1 and 3.2). For instance, with 10 µM H_2O_2 the residual As concentration (t = 30 min) was 4.8±0.2 µM (31% removal), which decreased to 1.7±0.1 µM (76% removal) with 40 µM

H_2O_2 (Fig. 3(A)). However, we also observed that increasing the H_2O_2 concentration above the amount required to completely oxidize 100±3 µM Fe(II) (i.e., over-dosage) also improved As(III) removal. For example, when the H_2O_2 dosage increased from 60 to 400 µM (i.e., over-dosage), the dissolved As concentration at t = 30 min decreased from 0.6±0.1 (92% removal) to 0.1±0.1 µM (98.5% removal), which resulted in As levels below the WHO recommended limit (<0.13 µM) (Fig. 3(A)). This increase in As removal can be explained by the oxidation of As(III) to As (V) via ROS, formed by decomposition of H_2O_2 on the surface of Fe(III) precipitates (Lin and Gurol, 1998), with subsequent sorption of As(V).

Finally, we noted that the removal of the initial 7±0.2 µM As(III) with 400 µM H_2O_2 (98.5% removal) was almost equal to the removal of the initial 7±0.5 µM As(V) (99.3% removal; at 60 µM H_2O_2), when a similar Fe dosage of 100±3 µM was used (Fig. 3(B)). This result highlights the advantage of using H_2O_2, because previous Fe(II)-based As removal studies, with only O_2 dosing, have always reported higher removals of initial As(V) compared to As(III) (Kumar et al., 2004; Roberts et al., 2004; Roy et al., 2020; Wan et al., 2011).
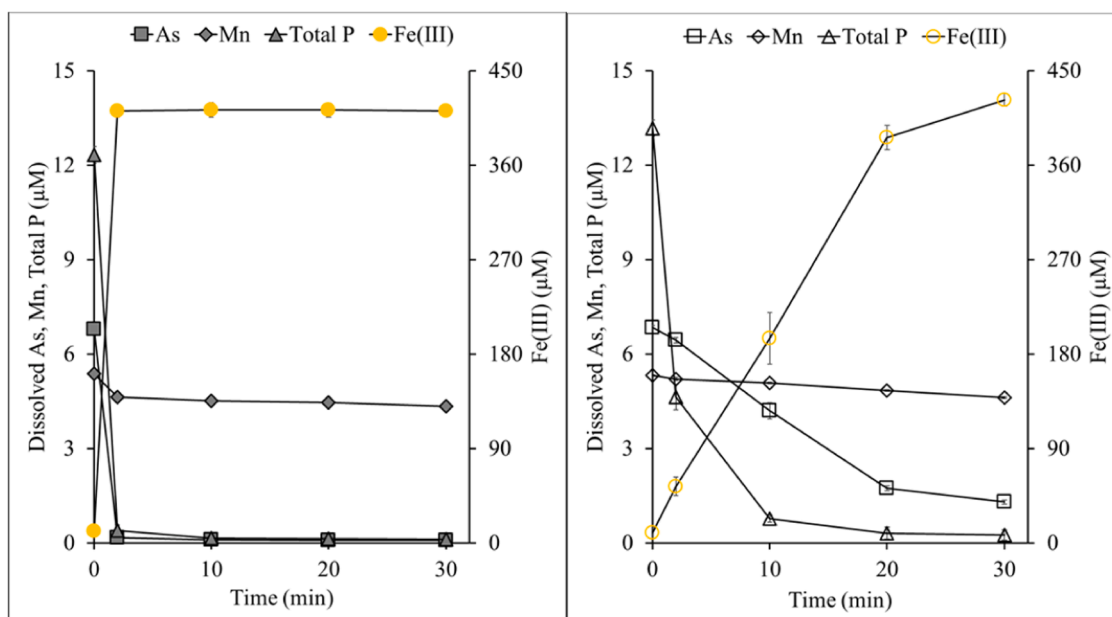
3.4. Application to raw anaerobic groundwater

To validate that enhanced As(III) co-removal can be achieved by adding H_2O_2 to groundwater containing native Fe(II), experiments were performed with raw anaerobic groundwater rich in Fe(II), co-occurring As(III), and other native dissolved species (such as phosphorous (total P) and manganese (Mn)). Fig. 4 shows the removal of initial As(III), Mn, and total P from raw anaerobic groundwater with Fe(III) generation over 30 min. Consistent with the laboratory experiments (Sections 3.1 and 3.2), all groundwater-native Fe(II) was oxidized with H_2O_2 and rapidly formed precipitates (within 2 min), whereas O_2 oxidation of Fe (II) required the full 30 min of the experiment. During the H_2O_2 dosing experiment, As(III) was also quickly removed, with 97.6% As(III) removal measured in 2 min. When the native Fe(II) in groundwater was oxidized by O_2, As(III) removal continued over the full 30 min reaction duration and at the end of the experiment 1.3±0.1 µM residual As (81% removal) remained in solution.

While our experiments with natural groundwater were consistent with the laboratory experiments (i.e., H_2O_2 addition outperformed
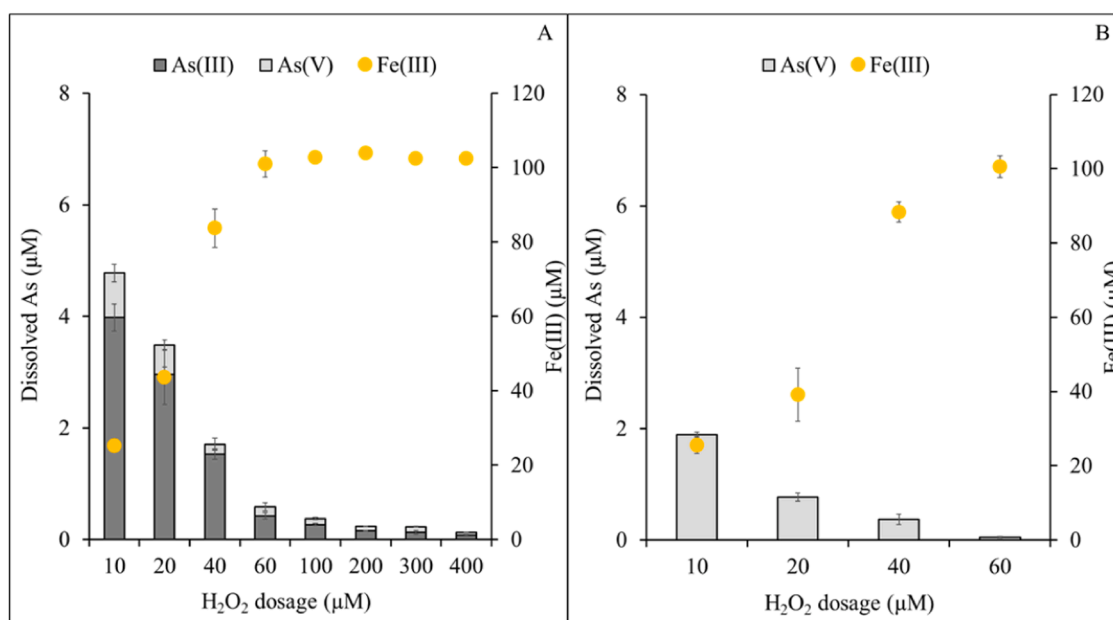
Fig. 3. Dissolved As and Fe(III) concentration in solutions at t = 30 min plotted as a function of different H_2O_2 dosage when 100±3 µM of Fe(II) was oxidized by 10-400 µM H_2O_2 anaerobically. Solutions initially contained 7±0.2 µM As(III) (A) or 7±0.5 µM As(V) (B), 2.5 mM NaHCO$_3$, and 10 mM NaCl. All Fe(III) formed solids and no dissolved Fe(III) was measured (data not shown). Data points and error bars represent the average and standard deviation of the samples obtained from replicate experiments.

Fig. 4. As, Mn, and total P removal from raw anaerobic groundwater as function of time and Fe(III) generation when 424 ± 12 μM groundwater-native Fe(II) was completely oxidized by 800 μM H_2O_2 (left) and 8.0-9.0 mg/L O_2 (right). Solutions initially contained 6.8 ± 0.1 μM As(III); 5.3 ± 0.1 μM Mn, and 12.7 ± 0.5 μM total P. All Fe(III) formed solids and no dissolved Fe(III) was measured (data not shown). Data points and error bars represent the average and standard deviation of the samples obtained from replicate experiments.

aeration), some key differences were observed. First, compared to the laboratory experiments, raw groundwater samples showed a better removal of As(III) for both H_2O_2 and O_2 oxidation. Second, the difference between As(III) removal using H_2O_2 or O_2 was smaller for the raw groundwater experiments. The less distinct As removal of H_2O_2 and O_2 oxidants applied to natural groundwater could be attributed to the four times higher Fe(II) concentration in natural groundwater than in the laboratory experiments, which suggests that optimal conditions for enhancing As removal by H_2O_2 addition occur at lower initial Fe(II) levels.

Additionally, the optimal removal of As(III) with H_2O_2 in groundwater containing low levels of native Fe(II) can also be impacted by the presence of other native species that can compete for adsorption sites and ROS. For example, phosphorous in groundwater is present mainly as phosphate (PO_4^{3-}) and studies have shown its competition with As(V) for adsorption sites on Fe solids (Roberts et al., 2004). As observed in Fig. 4, along with the removal of As(III), total P removal was also observed for both H_2O_2 and O_2 experiments, but the removal of total P was different for the different oxidants. In the O_2 experiment, the rate and amount of total P removal was higher than As(III), whereas the H_2O_2 experiment did not display a substantial difference between As(III) and total P removal. This result can be explained by the availability of sufficient sorption sites for both As and P on the Fe solids owing to the formation of poorly-ordered solids during H_2O_2 oxidation, the high Fe(II) concentration (424 ± 12 μM), and to the enhanced oxidation of As(III) using H_2O_2. However, in situations where native Fe(II) is low, a possible lower co-removal of As(III) could be expected due to competition with PO_4^{3-} for adsorption sites.

Apart from PO_4^{3-}, groundwater can also contain dissolved Mn, which might impact As(III) co-removal with native Fe(II). For instance, previous studies have reported that Mn in groundwater, which is present as Mn(II), can compete with As(III) for ROS, yielding oxidized Mn(III) that (partially) incorporates into the co-precipitating Fe(III) solids (Ahmad et al., 2019; Catrouillet et al., 2020; van Genuchten and Peña, 2017). However as shown in Fig. 4, Mn removal was relatively low for both H_2O_2 (19% removal) and O_2 (13% removal), suggesting that Mn(III) formation was not substantial. However, since identifying the solid-phase speciation of Mn was beyond the scope of this study, it is not

clear whether there was any competition between Mn(II) and As(III) for the generated ROS.

3.5. Implications for groundwater treatment

We observed improved As(III) removal when co-existing Fe(II) was oxidized by H_2O_2 rather than O_2. The ratio of As(III) removed to Fe(III) generated increased from 0.03 to 0.06 mol:mol when 100 μM Fe(II) was completely oxidized with either 8.0-9.0 mg/L O_2 or 100 μM H_2O_2, respectively, indicating substantially less Fe is required for equivalent As removal with H_2O_2. The application of such Fenton-type systems (i.e., Fe (II)+H_2O_2) to improve As(III) removal from water has been reported previously. For example, Krishna et al. (2001) showed that initial treatment of 2 mg/L As(III) with 100 mg/L Fe(II) and 100 μL/L of 30% H_2O_2, followed by passing through zero valent iron columns and a sand bed, achieved As removal to <10 μg/L (WHO guideline). In addition, Wang et al. (2013) observed that oxidizing 20 μM Fe(II) with 50 μM H_2O_2 at pH 7.0 resulted in 70% oxidation of 20 μM As(III) compared to just 2.5% while oxidizing the Fe(II) with O_2. While these studies are useful, they interpret their results primarily by improved As(III) co-oxidation by ROS and did not focus on the influence of Fe(III) precipitate structure. In this study, we also observed that the improved As (III) co-removal by H_2O_2 is partly attributed to the well-established enhanced efficiency of As(III) oxidation in Fe(II)+H_2O_2 systems due to higher stoichiometric yield of ROS compared to Fe(II)+O_2 systems (Bandaru et al., 2020; Hug and Leupin, 2003). However, our results explicitly showed that the Fe(III) precipitate structure played a major role in improving As(III) removal. The Fe K-edge EXAFS analysis performed in this study indicated a systematic decrease in precipitate crystallinity (i.e., increase in reactive specific surface area) from moderately crystalline Lp in the O_2 system to poorly-ordered Fe(III) precipitates with H_2O_2 (Fig. 1(C)). This impact of Fe(III) precipitate structure is often overlooked in Fe-based As removal techniques, but we show that the type of Fe(III) precipitates must be considered to accurately predict As removal in groundwater treatment.

Our results also indicated that oxidizing the groundwater-native Fe (II) anaerobically with H_2O_2 prior to aeration-filtration can be used to leverage the full potential of native Fe(II) for As(III) treatment.

Depending on the initial As:Fe and Fe:H$_2$O$_2$ ratios, this novel approach can remove As(III) to below drinking water standards, achieving a high As(III) removal, which is often difficult with conventional aeration-filtration. The optimal use of native Fe(II) via H$_2$O$_2$ oxidation can help to avoid the need for additional Fe dosage (as FeCl$_3$) in situations where oxidizing native Fe(II) by aeration is not sufficient to meet As drinking water limits. This reduction of Fe dosage will also lower the volume of generated Fe sludge and thus lower the frequency of filter backwashing. Additionally, anaerobic oxidation of Fe(II) with H$_2$O$_2$ prior to aeration will not result in the same increase in groundwater pH as is observed during aeration due to degassing of CO$_{2(g)}$. As long as Fe(II) is oxidized, maintaining a low pH is advantageous because As(V) adsorption to Fe solids decreases with increasing pH (Annaduzzaman et al., 2021b; Dixit and Hering, 2003).

Usage of other strong oxidants (such as KMnO$_4$ or NaOCl) during aeration-filtration has been reported previously, effectively oxidizing As(III) and also generating poorly-ordered Fe solids (van Genuchten and Ahmad, 2020). However, compared to those oxidants, H$_2$O$_2$ is considered a green oxidant, because its by-products, namely H$_2$O and O$_2$, are benign (Goyal et al., 2020; Pham et al., 2012b; Zhao et al., 2019). Recent studies have also shown that H$_2$O$_2$ can be electrochemically generated *in-situ* (Bandaru et al., 2020), which eliminates the necessity to maintain chemical stocks of H$_2$O$_2$ on site, thus decreasing the supply chain for operating groundwater treatment plants.

The results in this work suggest that oxidizing groundwater-native Fe(II) with H$_2$O$_2$ anaerobically prior to aeration-filtration can be a novel approach to optimize the co-removal of toxic As(III). However, our study did not take into account potentially different environmental scenarios that can impact As(III) removal. For example, the laboratory experiments were performed in controlled conditions with a fixed Fe(II):As(III) ratio and pH, and without the presence of other competing ions. While a set of experiments with raw anaerobic groundwater was performed, the advantage of oxidizing native Fe(II) with H$_2$O$_2$ over O$_2$ for As(III) co-removal diminished most likely due to the high concentration of native Fe(II). In the experiments with real groundwater, although 1 mol of H$_2$O$_2$ is sufficient to oxidize 2 mol of Fe(II), an excess H$_2$O$_2$ was dosed to minimize the impact of any atmospheric O$_2$ influx and to ensure complete oxidation of the native Fe(II) by H$_2$O$_2$ in absence of N$_{2(g)}$ dosage as in laboratory experiments. While our laboratory investigations and tests in real groundwater highlight the potential benefits of H$_2$O$_2$ dosing, it is recommended to perform further studies with real anaerobic groundwater under various environmental conditions, with optimization of the H$_2$O$_2$ dosage, to further validate the novelty of the proposed approach. Overall, the advantage of anaerobic H$_2$O$_2$ oxidation of native Fe(II) for As(III) removal is that it can be easily implemented in conventional or decentralized systems to treat As contaminated groundwater without major changes in infrastructure and without substantial increases in treatment costs.

Conclusions

In this study, we showed a novel approach where the co-removal of groundwater As(III) with native Fe(II) can be enhanced by oxidizing the Fe(II) anaerobically with H$_2$O$_2$ prior to aeration-filtration rather than conventionally by aeration (or O$_2$) under aerobic conditions. The enhanced As(III) co-removal with H$_2$O$_2$ was partly due to generation of a larger fraction of poorly-ordered Fe(III) solids with a higher reactive specific surface area compared to moderately crystalline Fe(III) solids generated by O$_2$ as well as the generation of more ROS per mole of Fe(II) when dosing H$_2$O$_2$ (1:1) compared to O$_2$ (1:3), thus favouring As(III) oxidation to readily adsorbed As(V). Hence, we propose the application of H$_2$O$_2$, a green oxidant, for anaerobic Fe(II) and As(III) co-oxidation in groundwater treatment prior to aeration to optimize native Fe(II) usage, which will reduce the volume of generated sludge.

CrediT authorship contribution statement

Mrinal Roy: Analysis Data, **Case M. van Genuchten**: Analysis Data, XAS analysis; guidance on design; for XAS, **Luuk Rietveld:** and guidance on design, **Doris van Halem:** guidance on design, Analysis Data

CRediT authorship contribution statement

Mrinal Roy: Conceptualization, Data curation, Investigation, Methodology, Visualization, Validation, Software, Writing – original draft. **Case M. van Genuchten:** Supervision, Conceptualization, Software, Visualization, Writing – review & editing. **Luuk Rietveld:** Supervision, Conceptualization, Writing – review & editing. **Doris van Halem:** Supervision, Conceptualization, Visualization, Writing – review & editing.

Declaration of Competing Interest

The authors declare that they have no known competing financial interests or personal relationships that could have appeared to influence the work reported in this paper.

Data availability

Data will be made available on request.

Supplementary materials

Supplementary material associated with this article can be found, in the online version, at doi:10.1016/j.watres.2022.119007.

References

Ahmad, A., van der Wal, A., Bhattacharya, P., van Genuchten, C.M., 2019. Characteristics of Fe and Mn bearing precipitates generated by Fe(II) and Mn(II) co-oxidation with O$_2$, MnO$_4$ and HOCl in the presence of groundwater ions. Water Res. 161 (June), 505–516. https://doi.org/10.1016/j.watres.2019.06.036.

Annaduzzaman, M., Bhattacharya, P., Biswas, A., Hossain, M., Ahmed, K.M., van Halem, D., 2018. Arsenic and manganese in shallow tubewells: validation of platform color as a screening tool in Bangladesh. Groundwater Sustain. Dev. 6, 181–188. https://doi.org/10.1016/J.GSD.2017.11.008.

Annaduzzaman, M., Rietveld, L.C., Ghosh, D., Hoque, B.A., van Halem, D., 2021a. Anoxic storage to promote arsenic removal with groundwater-native iron. Water Res. 202 https://doi.org/10.1016/J.WATRES.2021.117404.

Annaduzzaman, M., Rietveld, L.C., Hoque, B.A., Bari, M.N., van Halem, D., 2021b. Arsenic removal from iron-containing groundwater by delayed aeration in dual-media sand filters. J. Hazard. Mater. 411, 124823 https://doi.org/10.1016/J.JHAZMAT.2020.124823.

Bandaru, S.R.S., Van Genuchten, C.M., Kumar, A., Glade, S., Hernandez, D., Nahata, M., Gadgil, A., 2020. Rapid and efficient arsenic removal by iron electrocoagulation enabled with *in situ* generation of hydrogen peroxide. Environ. Sci. Technol. 54 (10), 6094–6103. https://doi.org/10.1021/acs.est.0c00012.

Bissen, M., Frimmel, F.H., 2003. Arsenic — a review. Part II: oxidation of arsenic and its removal in water treatment. Acta Hydroch. Hydrob. 31 (2), 97–107. https://doi.org/10.1002/AHEH.200300485.

Bora, A.J., Gogoi, S., Baruah, G., Dutta, R.K., 2016. Utilization of co-existing iron in arsenic removal from groundwater by oxidation-coagulation at optimized pH. J. Environ. Chem. Eng. 4 (3), 2683–2691. https://doi.org/10.1016/J.JECE.2016.05.012.

Catrouillet, C., Hirosue, S., Manetti, N., Boureau, V., Peña, J., 2020. Coupled As and Mn redox transformations in an Fe(0) electrocoagulation system: competition for

reactive oxidants and sorption sites. Environ. Sci. Technol. 54 (12), 7165–7174. https://doi.org/10.1021/acs.est.9b07099.

Dixit, S., Hering, J.G., 2003. Comparison of arsenic(V) and arsenic(III) sorption onto iron oxide minerals: implications for arsenic mobility. Environ. Sci. Technol. 37 (18), 4182–4189. https://doi.org/10.1021/ES030309T.

Goyal, R., Singh, O., Agrawal, A., Samanta, C., Sarkar, B., 2020. Advantages and limitations of catalytic oxidation with hydrogen peroxide: from bulk chemicals to lab scale process. Catal. Rev. Sci. Eng. 64 (2), 229–285. https://doi.org/10.1080/01614940.2020.1796190/FORMAT/EPUB.

Gude, J.C.J., Rietveld, L.C., van Halem, D., 2016. Fate of low arsenic concentrations during full-scale aeration and rapid filtration. Water Res. 88, 566–574. https://doi.org/10.1016/j.watres.2015.10.034.

Gude, J.C.J., Rietveld, L.C., van Halem, D., 2017. As(III) oxidation by MnO_2 during groundwater treatment. Water Res. 111, 41–51. https://doi.org/10.1016/j.watres.2016.12.041.

Gude, J.C.J., Rietveld, L.C., van Halem, D., 2018. Biological As(III) oxidation in rapid sand filters. J. Water Process Eng. 21, 107–115. https://doi.org/10.1016/j.jwpe.2017.12.003.

Holm, T.R., Wilson, S.D., 2006. Chemical oxidation for arsenic removal. MTAC Publ. TR06. -05.

Hug, S.J., Leupin, O., 2003. Iron-catalyzed oxidation of Arsenic(III) by oxygen and by hydrogen peroxide: pH-dependent formation of oxidants in the Fenton reaction. Environ. Sci. Technol. 37 (12), 2734–2742. https://doi.org/10.1021/es026208x.

Kapaj, S., Peterson, H., Liber, K., Bhattacharya, P., 2006. Human health effects from chronic arsenic poisoning - a review. J. Environ. Sci. Health - Part A Toxic/Hazard. Substances Environ. Eng. 41 (10), 2399–2428. https://doi.org/10.1080/10934520600873571.

King, D.W., 1998. Role of carbonate speciation on the oxidation rate of Fe(II) in aquatic systems. Environ. Sci. Technol. 32 (19), 2997–3003. https://doi.org/10.1021/ES980206O/SUPPL_FILE/ES980206O_S.PDF.

King, D.W., Farlow, R., 2000. Role of carbonate speciation on the oxidation of Fe(II) by H_2O_2. Mar. Chem. 70 (1–3), 201–209. https://doi.org/10.1016/S0304-4203(00)00026-8.

Krishna, M.V.B., Chandrasekaran, K., Karunasagar, D., Arunachalam, J., 2001. A combined treatment approach using Fenton's reagent and zero valent iron for the removal of arsenic from drinking water. J. Hazard. Mater. 84 (2–3), 229–240. https://doi.org/10.1016/S0304-3894(01)00205-9.

Kumar, P.R., Chaudhari, S., Khilar, K.C., Mahajan, S.P., 2004. Removal of arsenic from water by electrocoagulation. Chemosphere 55 (9), 1245–1252. https://doi.org/10.1016/j.chemosphere.2003.12.025.

Li, Y., Bland, G.D., Yan, W., 2016. Enhanced arsenite removal through surface-catalyzed oxidative coagulation treatment. Chemosphere 150, 650–658. https://doi.org/10.1016/j.chemosphere.2016.02.006.

Lin, S.S., Gurol, M.D., 1998. Catalytic decomposition of hydrogen peroxide on iron oxide: kinetics, mechanism, and implications. Environ. Sci. Technol. 32 (10), 1417–1423. https://doi.org/10.1021/es970648k.

Pedersen, H.D., Postma, D., Jakobsen, R., Larsen, O., 2005. Fast transformation of iron oxyhydroxides by the catalytic action of aqueous Fe(II). Geochim. Cosmochim. Acta 69 (16), 3967–3977. https://doi.org/10.1016/J.GCA.2005.03.016.

Pham, A.L.T., Doyle, F.M., Sedlak, D.L., 2012a. Inhibitory effect of dissolved silica on H_2O_2 decomposition by iron(III) and manganese(IV) oxides: implications for H_2O_2-based *in situ* chemical oxidation. Environ. Sci. Technol. 46 (2), 1055–1062. https://doi.org/10.1021/es203612d.

Pham, A.L.T., Doyle, F.M., Sedlak, D.L., 2012b. Kinetics and efficiency of H_2O_2 activation by iron-containing minerals and aquifer materials. Water Res. 46 (19), 6454–6462. https://doi.org/10.1016/J.WATRES.2012.09.020.

Podgorski, J., Berg, M., 2020. Global threat of arsenic in groundwater. Science 368 (6493), 845–850. https://doi.org/10.1126/science.aba1510.

Roberts, L.C., Hug, S.J., Ruettimann, T., Billah, M., Khan, A.W., Rahman, M.T., 2004. Arsenic removal with iron(II) and iron(III) in waters with high silicate and phosphate concentrations. Environ. Sci. Technol. 38 (1), 307–315. https://doi.org/10.1021/es0343205.

Roy, M., van Genuchten, C.M., Rietveld, L., van Halem, D., 2020. Integrating biological As(III) oxidation with Fe(0) electrocoagulation for arsenic removal from groundwater. Water Res. 188, 116531 https://doi.org/10.1016/j.watres.2020.116531.

Sharma, A.K., Sorlini, S., Crotti, B.M., Collivignarelli, M.C., Tjell, J.C., Abbà, A., 2016. Enhancing arsenic removal from groundwater at household level with naturally occurring iron. Rev. Ambiente Água 11 (3), 486–498. https://doi.org/10.4136/AMBI-AGUA.1815.

Toner, B.M., Santelli, C.M., Marcus, M.A., Wirth, R., Chan, C.S., McCollom, T., Bach, W., Edwards, K.J., 2009. Biogenic iron oxyhydroxide formation at mid-ocean ridge hydrothermal vents: Juan de Fuca Ridge. Geochim. Cosmochim. Acta 73 (2), 388–403. https://doi.org/10.1016/j.gca.2008.09.035.

Tseng, W.P., 1977. Effects and dose response relationships of skin cancer and blackfoot disease with arsenic. Environ. Health Perspect. Vol.19, 109–119. https://doi.org/10.1289/ehp.7719109.

van Genuchten, C.M., Behrends, T., Kraal, P., Stipp, S.L.S., Dideriksen, K., 2018. Controls on the formation of Fe(II,III) (hydr)oxides by Fe(0) electrolysis. Electrochim. Acta 286, 324–338. https://doi.org/10.1016/j.electacta.2018.08.031.

van Genuchten, C M, Pena, J., 2017. Mn(II) oxidation in fenton and fenton type systems: identification of reaction efficiency and reaction products. Environ. Sci. Technol. 51 (5), 2982–2991. https://doi.org/10.1021/acs.est.6b05584.

van, Genuchten, Case, M., Addy, S.E.A., Peña, J., Gadgil, A.J., 2012. Removing arsenic from synthetic groundwater with iron electrocoagulation: an Fe and As K-edge EXAFS study. Environ. Sci. Technol. 46 (2), 986–994. https://doi.org/10.1021/es201913a.

van, Genuchten, Case, M., Ahmad, A., 2020. Groundwater as removal by As(III), Fe(II), and Mn(II) Co-oxidation: contrasting as removal pathways with O_2, NaOCl, and $KMnO_4$. Environ. Sci. Technol. 54 (23), 15454–15464. https://doi.org/10.1021/acs.est.0c05424.

van, Genuchten, Case, M, Gadgil, A.J., Peña, J., 2014. Fe(III) nucleation in the presence of bivalent cations and oxyanions leads to subnanoscale 7 Å polymers. Environ. Sci. Technol 48 (21). https://doi.org/10.1021/es503281a.

Wan, W., Pepping, T.J., Banerji, T., Chaudhari, S., Giammar, D.E., 2011. Effects of water chemistry on arsenic removal from drinking water by electrocoagulation. Water Res. 45 (1), 384–392. https://doi.org/10.1016/j.watres.2010.08.016.

Wang, Z., Bush, R.T., Liu, J., 2013. Arsenic(III) and iron(II) co-oxidation by oxygen and hydrogen peroxide: divergent reactions in the presence of organic ligands. Chemosphere 93 (9), 1936–1941. https://doi.org/10.1016/j.chemosphere.2013.06.076.

Webb, S.M., 2005. SIXpack: a graphical user interface for XAS analysis using IFEFFIT. Phys. Scr. T T115 (T115), 1011–1014. https://doi.org/10.1238/Physica.Topical.115a01011.

Zhao, H., Li, Z., Jin, J., 2019. Green oxidant H_2O_2 as a hydrogen atom transfer reagent for visible light-mediated Minisci reaction. New J. Chem. 43 (32), 12533–12537. https://doi.org/10.1039/C9NJ03106E.